Solution Properties of Amylose Tris(Phenylcarbamate): Local Conformation and Chain Stiffness in 1,4-Dioxane and 2-Ethoxyethanol

By Ken TERAO,[1,] Taichi FUJII,[1] Maiko TSUDA,[1] Shinichi KITAMURA,[2] and Takashi NORISUYE[1]*

[1]Department of Macromolecular Science, Graduate School of Science, Osaka University, 1-1, Machikaneyama-cho, Toyonaka, Osaka 560-0043, Japan

[2]Graduate School of Life and Environmental Sciences, Osaka Prefecture University, Gakuen-cho, Nakaku, Sakai, Osaka 599-8531, Japan

*To whom correspondence should be addressed (Tel:+81-6-6850-5459, FAX:+81-6- 6850-5461, E-mail: kterao@chem.sci.osaka-u.ac.jp).

RUNNING HEAD: Solution Properties of Amylose Tris(Phenylcarbamate)

ABSTRACT: Light and small-angle X-ray scattering, sedimentation equilibrium, viscosity, circular dichroism, and infrared absorption measurements have been made on 1,4-dioxane (DIOX) and 2-ethoxyethanol (2EE) solutions of seven amylose tris(phenylcarbamate) samples ranging in molecular weight from 2×10^4 to 3×10^6. Analyses of gyration radius, scattering function, and intrinsic viscosity data in terms of the wormlike chain model yield Kuhn segment lengths of 22 ± 2 nm and 16 ± 2 nm in DIOX and 2EE, respectively, and a contour length per residue of 0.33 ± 0.02 nm in both, showing that the amylose derivative chain has high stiffness and a contour length slightly shorter than the known value 0.37 - 0.40 nm for amylosetriesters in the crystalline state. These results are consistent with the intramolecular hydrogen bonding between the C=O and NH groups of the neighbor repeating units detected by infrared absorption and also with the locally regular (or helical) conformation indicated by circular dichroism.

KEY WORDS: Amylose Tris(Phenylcarbamate) / Light Scattering / SAXS / Intrinsic Viscosity / Wormlike Chain / Hydrogen Bonding

Dilute solutions of amylose tris(phenylcarbamate) (ATPC), whose chemical structure is illustrated in Figure 1, have widely been studied due to the good solubility in various solvents including some theta solvents.[1-12] This derivative behaves as a stiff chain in solution in contrast to the high flexibility of amylose.[13,14] The contrast suggests that intramolecular hydrogen bonding between neighboring C=O and NH groups is responsible for the stiffness of the ATPC chain. If indeed formed, such hydrogen bonds should affect the local conformation of ATPC and the contour length h per repeat unit, *i.e.*, the helix pitch per residue (provided the chain is helical), in addition to the global conformation or the chain stiffness. The local structure of this amylose derivative is also a subject in efficient chiral separation.[15,16]

[Figure 1]

Despite such importance of h, however, we find no report on its experimental determination for ATPC in the literature except the very early work of Burchard,[8] who, analyzing gyration radius data in terms of the wormlike chain,[17] estimated h in the dioxane-methanol mixed theta solvent to be 0.26 nm, a value about one-half that of cellulose tris(phenylcarbamate). The Kuhn segment length λ^{-1} he obtained was as large as 46 nm. Later, in their characterization work on ATPC, Pfannemüller et al.[11] estimated λ^{-1} to be 18 – 26 nm in 1,4-dioxane (DIOX) assuming h = 0.37 nm (the helix pitch per residue based on the crystal structure of amylose tribenzoate[18]). These estimates of λ^{-1} by the two groups are at variance depending strongly on h.

For the understanding of the conformational characteristics, local and global, of ATPC in solution, unequivocal determination of the wormlike-chain parameters (h and λ^{-1}) is almost mandatory in a solvent in which intramolecular hydrogen bonds between C=O and NH groups are detected by experiment. Thus, in the present work, we made light scattering, sedimentation equilibrium, synchrotron radiation small-angle X-ray

scattering (SAXS), viscosity, circular dichroism (CD), and infrared absorption (IR) measurements on ATPC samples in DIOX and 2-ethoxyethanol (2EE). These solvents allowed us to obtain information on the (possible) helical conformation of the ATPC molecule and the intramolecular hydrogen bonding from CD and IR, respectively. The estimation of the wormlike-chain parameters from scattering and viscosity data are described below along with these findings from spectroscopy.

EXPERIMENTAL

Preparation of ATPC Samples

Seven amylose samples with narrow molecular-weight distribution and no branching[19-22] were enzymatically synthesized by the previously reported method[19] using potato phosphorylase (EC 2.4.1.1.) or supplied by Ezaki Glico Co., Ltd. Their weight-average molecular weights M_w ranged from 6×10^3 to 1×10^6 and their weight to number-average molecular weight ratios M_w/M_n were less than 1.2 when estimated by SEC-LS (size exclusion chromatography combined with multi-angle or low-angle light scattering and refractometry). ATPC samples were synthesized from the amylose samples and phenylisocyanate. The typical procedures were as follows.

Each amylose sample (3.0 g) and LiCl (3.0 g) dried in vacuum at 130 °C for several hours were dissolved in *N*,*N*'-dimethylacetoamide (30 cm^3) at 110 °C under N_2 atmosphere. Pyridine (100 cm^3) and an excess amount (20 g, 0.17 mol) of phenylisocyanate were added to the mixture and stirred for 12 h at 110 °C. The product was reprecipitated twice from an acetone solution into methanol to remove foreign substances such as unreacted phenylisocyanate and LiCl. LiCl and phenylisocyanate (Wako and Tokyo Kasei, respectively) were used without further purification. *N*,*N*'-dimethylacetoamide, pyridine, DIOX, and 2EE (Wako) were

purified by fractional distillation over CaH_2.

The resultant samples were further purified by fractional precipitation with acetone as a solvent and methanol as a precipitant, and appropriate middle fractions from the respective ATPC samples were reprecipitated into methanol. They were designated as ATPC20K, ATPC50K, ATPC200K, ATPC300K, ATPC500K, ATPC800K, and ATPC3M based on the molecular weights. The degree of substitution was estimated to be 3.0 - 3.1 for all these fractions from the mass ratio of carbon to nitrogen determined by elemental analysis. It was also determined for ATPC20K and ATPC50K to be 3.0 ± 0.1 by ^{1}H NMR (JEOL GSX-400 NMR spectrometer) in acetone-d_6 at 30 °C. Thus we concluded that the three hydroxyl groups on each glucose unit of amylose were fully substituted to phenylcarbamate.

Light Scattering

Light scattering measurements were made for five high molecular weight ATPC samples in DIOX and 2EE at 25°C on a Fica-50 light scattering photometer with vertically polarized incident light of 436 or 546-nm wavelength λ_0 in an angular range from 22.5° to 150°. The instrument was calibrated with benzene at 25 °C with the Rayleigh ratio for the unpolarized incident light at 90° taken as 4.65×10^{-5} cm^{-1} at 436 nm and 1.61×10^{-5} cm^{-1} at 546 nm;[23] the depolarization ratio of this liquid was determined to be 0.44 and 0.41 for 436 and 546 nm, respectively, by the method of Rubingh and Yu.[24]

The square-root plots[25] of $(Kc/R_\theta)^{1/2}$ *vs.* $\sin^2(\theta/2)$ and *vs.* c were used to determine M_w, the second virial coefficient A_2, and the z-average mean-square radius of gyration $\langle S^2 \rangle_z$, where K, c, and R_θ denote the optical constant, the polymer mass concentration, and the excess reduced scattering intensity at scattering angle θ, respectively.

Polymer solutions and the solvents were made optically clean by centrifugation at about 3×10^4 gravities for 80 minutes at 25°C. Each of them was transferred into a cylindrical light scattering cell (22 mm i.d.) with a stainless steel tube (0.5 mm i.d.). The cell and the tube had been cleaned by acetone filtered through a 0.02 μm membrane filter.

The specific refractive index increments $\partial n/\partial c$ for ATPC20K and ATPC3M in DIOX and for ATPC800K in 2EE at 25°C were determined using a modified Schulz-Cantow type differential refractometer. The results at λ_0 = 436, 546, and 633 nm were 0.160, 0.148, 0.143 cm^3g^{-1}, respectively, for ATPC3M in DIOX; the values for ATPC20K in DIOX were about 2% larger than these at the corresponding wavelengths. For ATPC800K in 2EE, we obtained $\partial n/\partial c$ = 0.173, 0.159, 0.153 cm^3g^{-1} for λ_0 = 436, 546, and 633 nm, respectively.

Small-angle X-ray scattering (SAXS)

Scattering intensities at θ and at λ_0 = 0.10 nm were measured for ATPC20K and ATPC50K both in DIOX and in 2EE at 25 °C using a Rigaku R-AXIS IV++ or an R-AXIS VII imaging plate detector at the BL40B2 beamline in SPring-8; the camera length was set to be 1500 mm. A 1.5 mmϕ quartz capillary filled with each test solution was set to the cell holder whose temperature was controlled with a circulating waterbath. The beam center of the imaging plate and the camera length were determined accurately from the Bragg reflection of powdery lead stearate. The scattering intensities for each solution or solvent were corrected for the incident-beam intensity and the transmittance, both determined using the ionic chambers installed at the upper and lower ends of the capillary. The excess scattering intensity I_θ was analyzed using the square-root plots[25] of $(c/I_\theta)^{1/2}$ *vs.* $\sin^2(\theta/2)$ and *vs.* c to determine

$\langle S^2 \rangle_z$ and $P(k)$ (the particle scattering function) at the absolute value of the scattering vector k.

Sedimentation Equilibrium

Sedimentation equilibrium measurements were made for samples ATPC20K and ATPC50K in DIOX at 25 °C in a Beckman Optima XL-I analytical ultracentrifuge to determine M_w, A_2, and the z-average molecular weight M_z (see ref 26 for the experimental procedures and data analysis). The rotor speed was chosen to be 3×10^4 and 1.1×10^4 rpm for ATPC20K and ATPC50K, respectively. The concentration profile in each 12-mm double sector cell was obtained from the Rayleigh interference patterns observed with a diode laser of $\lambda_0 = 675$ nm. The $\partial n/\partial c$ at this λ_0 was estimated from the above-mentioned data at other λ_0 with the aid of $\partial n/\partial c$ *vs.* λ_0^{-2} plot. The partial specific volume was determined for ATPC20K and ATPC50K in DIOX at 25 °C to be 0.714 and 0.724 cm^3g^{-1}, respectively, using an Anton Paar DMA 5000 densitometer.

Viscometry

Viscosity measurements in DIOX and in 2EE at 25 °C were carried out using a four-bulb low-shear capillary viscometer of the Ubbelohde type for ATPC3M in DIOX and conventional capillary viscometers for all ATPC samples in the two solvents. The Huggins plot,[27] the Fuoss-Mead plot,[28] and the Billmeyer plot[29] were combined to determine the intrinsic viscosity $[\eta]$ and the Huggins constant k'. The shear-rate effect on $[\eta]$ was negligible (less than 2%) even for the highest M_w sample ATPC3M.

Circular Dichroism

Both CD and UV spectra for ATPC300K in DIOX and in 2EE at 25 °C were recorded on a JASCO J720WO spectropolarimeter in the range of λ_0 between 210 and 280 nm. The experimental conditions were as follows: a band-width of 10 nm, a response time of 2 sec, a scanning rate of 20 nm / min, and five times accumulations. A rectangular quartz cell of 2-mm path length (l) was set in a cell holder thermostated with a circulating waterbath. The molar extinction coefficient ε and the molar circular dichroism $\Delta\varepsilon$ were calculated from the measured absorbance A and ellipticity θ' with

$$\varepsilon = \frac{AM_0}{cl}, \quad \Delta\varepsilon = \frac{\theta' M_0}{33cl} \tag{1}$$

where M_0 denotes the molar mass of the repeating unit of ATPC.

Infrared Absorption (IR)

IR spectra for ATPC300K in mixtures of DIOX and 2EE with different compositions were recorded on a Excalibur FTS-300 Fourier-transform infrared spectrometer (Bio Rad Laboratories) with a solution cell SC-CaF-0.05 (GL Science, Japan) made of CaF_2 and having 0.05-mm path length. The conventional transmission method was used, and 500 times accumulations were performed at room temperature (20 – 25 °C) for each solution whose c was about 3×10^{-2} g cm^{-3}. Additional measurements in pure DIOX and 2EE at higher polymer concentrations of about 6×10^{-2} g cm^{-3} gave spectra (A relative to c) identical to those at $c \sim 3 \times 10^{-2}$ g cm^{-3}, indicating negligible contributions from intermolecular interactions between polymer chains to IR spectra at c below 6×10^{-2} g cm^{-3}.

RESULTS

Dimensional and Hydrodynamic Properties

Figure 2 illustrates the concentration dependence of $(Kc/R_0)^{1/2}$ for ATPC samples in the two solvents, where R_0 denotes R_θ at $\theta = 0$. The indicated straight lines give A_2 values of 1 - 4 × 10^{-4} mol cm^3g^{-2}, showing that both DIOX and 2EE are good solvents for ATPC. The values of M_w determined in the two solvents agree with each other within ±3%, so that their averages are presented in Table I, along with the A_2 data. The table also includes M_w and M_z/M_w from sedimentation equilibrium as well as M_w/M_n determined by SEC-LS in tetrahydrofuran at 30 °C.

[Figure 2]

The angular dependence of $P(k)^{-1/2}$ is shown in Figure 3, in which the initial slopes indicated by the dashed lines and hence the radii of gyration for the respective samples are seen to be larger in DIOX than in 2EE. The values of $\langle S^2\rangle_z^{1/2}$ determined are listed in Table I.

[Figure 3], [Table I]

Figure 4 displays the M_w-dependence of $\langle S^2\rangle_z^{1/2}$ and $[\eta]$ in DIOX at 25 °C, along with the relations reported by Burchard[3] and Pfannemüller et al.[11] The $[\eta]$ data of the three groups come fairly close to one another, whereas Burchard's $\langle S^2\rangle_z$ data appear slightly above ours. The slopes of the curves fitting our $\langle S^2\rangle_z^{1/2}$ and $[\eta]$ data decrease from 0.74 to 0.55 and from 0.89 to 0.68, respectively, with increasing M_w, confirming the stiff-chain behavior of ATPC. These physical properties in 2EE exhibit similar behavior (see Figures 7 and 9). Our numerical results of $[\eta]$ and k' in DIOX and 2EE have been summarized in Table I.

[Figure 4]

IR and CD Spectra

Figure 5a illustrates IR spectra for ATPC300K in mixtures of DIOX and 2EE with indicated volume fractions x of 2EE. We assigned the double peaks at 1706 and 1754 cm^{-1} to the amide I band[30] which depends remarkably on x while the other peaks are almost independent of x. The amide I band reflects C=O stretching, and the double peaks indicate the presence of, at least, two different C=O groups in solution, that is, intramolecularly hydrogen bonding C=O with NH (1706 cm^{-1}; roughly 40% in amount) and virtually no or weakly interacting C=O with some species (1754 cm^{-1}). As x increases, the peak height at the latter band lowers as a result of the appearance of a new peak between the two peaks. The third peak at 1725 cm^{-1} is clearly visible in the difference spectra (Figure 5b) obtained by subtracting ε in DIOX ($\varepsilon_{(\text{in DIOX})}$) from those in the indicated solvents. This new peak is most likely due to the formation of hydrogen bonds –C=O---$HOC_2H_4OC_2H_5$. On the other hand, the shape and height of the peak at 1706 cm^{-1} are almost independent of x, indicating that the intramolecular hydrogen bonding is hardly affected by the presence of the hydroxyl group of 2EE. We may conclude from these findings that on an average, about 40% of the C=O groups in the ATPC molecule intramolecularly hydrogen bond to NH groups probably in the first and/or second nearest neighbor repeat units.

[Figure 5]

Figure 6 shows that there is no substantial difference in CD and UV spectra between the two solvents. Thus the local conformations of ATPC in DIOX and 2EE must be essentially the same. The pronounced positive maximum and negative minimum around λ_0 = 225 and 240 nm, respectively, may be taken to indicate that, as proposed by Bittiger and Keilich,[4] the ATPC molecule should have locally regular or

helical structure in the two solvents.

[Figure 6]

DISCUSSION

Analysis of Scattering Data

The unperturbed mean-square radius of gyration $\langle S^2 \rangle_0$ of a wormlike chain may be expressed as[31]

$$\left\langle S^2 \right\rangle_0 = \frac{L}{6\lambda} - \frac{1}{4\lambda^2} + \frac{1}{4\lambda^3 L} - \frac{1}{8\lambda^4 L^2}\left[1 - \exp(-2\lambda L)\right] \qquad (2)$$

where the contour length L of the chain is related to the molar mass M by

$$L = M/M_L \qquad (3)$$

with M_L being the molar mass per unit contour length. In the framework of the quasi-two-parameter (QTP) theory[32-34] with the Domb-Barrett equation[35] for the radius expansion factor α_s, $\langle S^2 \rangle$ ($\equiv \langle S^2 \rangle_0 \alpha_s^2$) is described by L, λ^{-1}, and the excluded-volume strength B. These three parameters were determined by the trial and error method to be $M_L = 1550 \pm 70$ nm^{-1}, $\lambda^{-1} = 24 \pm 3$ nm, and $B = 1 \pm 1$ nm in DIOX and $M_L = 1590 \pm 70$ nm^{-1}, $\lambda^{-1} = 18 \pm 2$ nm, and $B = 0.8 \pm 0.8$ nm in 2EE. In Figure 7, the calculated solid curves are seen to closely fit the data points. The excluded-volume effect in either solvent, that is, the difference between the solid and dashed curves, is quite small (less than 5%) even at the highest M_w investigated.

[Figure 7]

Nakamura and Norisuye's theory[36] for $P(k)$ of an unperturbed wormlike cylinder was applied to the SAXS data for ATPC50K, yielding M_L = 1540 nm^{-1}, λ^{-1} = 21 nm, and d = 1.3 nm in DIOX and M_L = 1640 nm^{-1}, λ^{-1} = 15 nm, and d = 1.4 nm in 2EE. The calculated solid lines of $kP(k)$ almost quantitatively reproduce the angular dependence of the experimental data, as shown in the two upper panels of Figure 8. The dashed curves calculated for the rod limit ($\lambda^{-1} = \infty$) considerably differ from the solid ones around k = 0.3 nm^{-1}. For ATPC20K, we obtained M_L = 1500 nm^{-1} and d = 1.3 nm in DIOX and M_L = 1580 nm^{-1} and d = 1.6 nm in 2EE by assuming the above λ^{-1} values for ATPC50K; we note that λ^{-1} cannot be determined for ATPC20K because the theoretical solid lines fitting the data points in the two lower panels of the figure are hardly distinguishable from the corresponding dashed lines for the rod limit. In sum, the wormlike-chain parameters estimated from $P(k)$ (M_L = 1520 ± 20 nm^{-1}, λ^{-1} = 21 nm, and d = 1.3 nm in DIOX and M_L = 1610 ± 30 nm^{-1}, λ^{-1} = 15 nm, and d = 1.5 ± 0.1 nm in 2EE) essentially agree with those from $\langle S^2 \rangle_z$ in the corresponding solvents. We note that the contribution $d^2/8$ from the chain thickness to $\langle S^2 \rangle$ of the cylindrical wormlike chain[37] is at most 3.1% and hence negligible.

[Figure 8]

Analysis of [η] Data

The intrinsic viscosity of a perturbed wormlike cylinder is given by the product of the unperturbed intrinsic viscosity $[\eta]_0$ and the cubic viscosity expansion factor α_η^3. The former, formulated by Yamakawa and Yoshizaki,[38] may be expressed as

$$[\eta]_0 = \frac{f(\lambda L, \lambda d)}{\lambda^3 M} \qquad (4)$$

For the latter, we use the Barrett equation[39] in the QTP scheme, so that the four parameters, M_L, λ^{-1}, d, and B, characterize $[\eta]$.

We analyzed the present $[\eta]$ data with M_L fixed to the mean from $P(k)$ and $\langle S^2 \rangle_z$ (1540 and 1600 nm^{-1} in DIOX and 2EE, respectively); we note that the four parameters cannot uniquely be determined from the $[\eta]$ data. Figure 9 shows the molecular weight dependence of experimental $[\eta]$ to be almost quantitatively reproduced by the solid curves calculated with λ^{-1} = 20 (± 1) nm, d = 2.9 (± 0.1) nm, and B = 0.5 (± 0.5) nm in DIOX and λ^{-1} = 14 (± 1) nm, d = 2.8 (± 0.1) nm, and B = 0.3 (± 0.3) nm in 2EE; each bracketed value indicates the uncertainty. The λ^{-1} values in the two solvents are in substantial agreement with those determined from $P(k)$ and $\langle S^2 \rangle_z$. The discrepancy between the hydrodynamic d from $[\eta]$ (2.8 - 2.9 nm) and the statistical d from $P(k)$ (1.3 - 1.5 nm) may be taken to reflect the electron density profile around the ATPC chain contour in solution.[34,40,41]

[Figure 9]

Chain Stiffness and Local Conformation

The wormlike-chain parameters obtained from the three physical properties, $\langle S^2 \rangle_z$, $P(k)$, and $[\eta]$, are summarized in Table II, where h has been calculated from $h = M_0 / M_L$. The values of λ^{-1} (the Kuhn length or more generally the stiffness parameter in the helical wormlike chain[34]) in the two solvents are much larger than that for amylose in dimethylsulfoxide (λ^{-1} = 4 nm) and comparable to that for cellulose tris(phenylcarbamate) in tetrahydrofuran (λ^{-1} = 21 nm).[42] This high stiffness of ATPC compared to amylose may be ascribed to the intramolecular hydrogen bonding between the C=O and NH groups as well as the high substituent density. The present IR

spectra (Figure 5a) demonstrate the presence of intramolecular hydrogen bonds in DIOX and 2EE. Since the proton donor ability of the latter solvent is higher than that of the former, we may interpret the slightly smaller λ^{-1} in 2EE as due to fewer intramolecular hydrogen bonds between the NH and C=O groups of ATPC. However, such a subtle difference in hydrogen bonding cannot be observed from the present IR spectra. On the other hand, the exciton splitting in the CD spectra of ATPC (Figure 6) substantiates the significance of the substituent effect because the CD spectra indicate the dense and regularly (or helically) allocated phenyl groups near the main chain.

[Table II]

The estimated values of h in DIOX and 2EE in Table II are substantially the same and both (0.33 ± 0.02 nm) are smaller than 0.37 - 0.40 nm known for amylosetriesters in the crystalline state.[18,43] This seems consistent with the IR and CD spectra showing the presence of intramolecular hydrogen bonds and locally regular structure. It should be noted that the h values in the two solvents can be smaller by about 10% if the polydispersity correction is made for $\langle S^2 \rangle_z$ with $M_z/M_w \sim 1.1$.

Conformational energy maps for both amylose[44,45] and amylose tris(3,5-dimethylphenylcarbamate)[46] have a shallow minimum which allows the left handed helices with various h values. This indicates that h of the amylosic chain may be influenced by a small perturbation, *i.e.*, intramolecular hydrogen bonding, intermolecular hydrogen bonding with solvent molecules, and packing of substituents and solvent molecules, and thus must be susceptible to such effects. Nonetheless, we find that the h values for ATPC in the two solvents happen to be essentially the same. It is intriguing to investigate h of ATPC in various solvents and also of other amylose derivatives in relation to their local conformation and chain stiffness.

CONCLUSIONS

The contour length *h* per repeating unit for amylose tris(phenylcarbamate) (ATPC) is 0.33 ± 0.02 nm in 1,4-dioxane (DIOX) and in 2-ethoxyethanol (2EE). This value is 10-20% smaller than those for amylosetriesters probably due to the intramolecular hydrogen bonding between C=O and NH groups of the neighbor glucose units, detected from the split amide I band. The locally regular or helical conformations as indicated by CD are essentially the same in the two solvents. The Kuhn segment length (or more generally the stiffness parameter in the helical wormlike chain) is much higher (22 ± 2 nm in DIOX and 16 ± 2 nm in 2EE) than that (4 nm) of amylose in dimethylsulfoxide due to the combination effect of the intramolecular hydrogen bonding and high segment density of phenyl carbamate groups.

Acknowledgment. We are grateful to Professors Kenji Okuyama (Osaka University) and Yo Nakamura (Kyoto University) for their help in SAXS measurements and data analysis, Professor Tadashi Inoue (Osaka University) for FT-IR measurements, and Professor Takahiro Sato (Osaka University) for fruitful discussions. We also thank Ezaki Glico Co. for providing amylose samples. The synchrotron radiation experiments were performed at the BL40B2 in SPring-8 with the approval of the Japan Synchrotron Radiation Research Institute (JASRI) (Proposal #2007A1034 and #2007B1296).

REFERENCES

1. W. Burchard, *Z. Physik. Chem.*, **42**, 293 (1964).

2. J. M. G. Cowie, *Biopolymers*, **3**, 69 (1965).

3. W. Burchard, *Makromol. Chem*., **88**, 11 (1965).

4. H. Bittiger and G. Keilich, *Biopolymers*, **7**, 539 (1969).

5. W. Banks, C. T. Greenwood, and J. Sloss, *Makromol. Chem.*, **140**, 109 (1970), *ibid*. **140**, 119 (1970).

6. W. Banks and C. T. Greenwood, *Makromol. Chem.*, **144**, 135 (1971).

7. W. Banks, C. T. Greenwood, and J. Sloss, *Eur. Polym. J.*, **7**, 879 (1971).

8. W. Burchard, *Br. Polym. J.*, **3**, 214 (1971).

9. W. Sutter and W. Burchard, *Makromol. Chem*., **179**, 1961 (1978).

10. A. K. Gupta, E. Marchal, W. Burchard, and B. Pfannemüller, *Macromolecules*, **12**, 281 (1979).

11. B. Pfannemüller, M. Schmidt, G. Ziegast, and K. Matsuo, *Macromolecules*, **17**, 710 (1984).

12. Y. Muroga, K. Hayashi, M. Fukunaga, T. Kato, S. Shimizu, and K. Kurita, *Biophys. Chem*., **121**, 96 (2006).

13. Y. Nakanishi, T. Norisuye, A. Teramoto, and S. Kitamura, *Macromolecules*, **26**, 4220 (1993).

14. T. Norisuye, *Polym. J*., **26**, 1303 (1994).

15. Y. Okamoto and E. Yashima, *Angew. Chem. Int. Ed*., **37**, 1020 (1998).

16. C. Yamamoto and Y. Okamoto, *Bull. Chem. Soc. Jpn*., **77**, 227 (2004).

17. O. Kratky and G. Porod, *Recl. Trav. Chim. Pays-bas*, **68**, 1106 (1949).

18. P. Zugenmaier and H. Steinmeier, *Polymer*, **27**, 1601 (1986).

19. S. Kitamura, H. Yunokawa, S. Mitsuie, and T. Kuge, *Polym. J*., **14**, 93 (1982).

20. S. Kitamura, K. Kobayashi, H. Tanahashi, T. Ozaki, and T. Kuge, *Denpun Kagaku (J. Jpn. Soc. Starch Sci.)* **36**, 257 (1989).

21. S. Kitamura, in "The Polymeric Materials Encyclopedia, Synthesis, Properties and Applications," J. C. Salamone, Ed.; CRC Press: New York, 1996; Vol. 10, p 7915.

22. H. Waldmann, D. Gygax, M. D. Bednarski, W. R. Shangraw, and G. M. Whitesides, *Carbohydr. Res*., **157**, C4 (1986).

23. Gj. Deželić and J. Vavra, *Croat. Chem. Acta*, **38**, 35 (1966).

24. D. N. Rubingh and H. Yu, *Macromolecules*, **9**, 681 (1976).

25. G. C. Berry, *J. Chem. Phys*., **44**, 4550 (1966).

26. T. Norisuye, T. Yanaki, and H. Fujita, *J. Polym. Sci. Polym: Phys. Ed*., **18**, 547 (1980).

27. M. L. Huggins, *J. Am. Chem. Soc.*, **64**, 2716 (1942).

28. D. F. Mead and R. M. Fuoss, *J. Am. Chem. Soc.*, **64**, 277 (1942).

29. F. W. Billmeyer Jr., *J. Polym. Sci.*, **4**, 83 (1949).

30. R. B. Kasat, Y. Zvinevich, H. W. Hillhouse, K. T. Thomson, N.-H. L. Wang, and E. I. Franses, *J. Phys. Chem. B.*, **110**, 14114 (2006).

31. H. Benoit and P. Doty, *J. Phys. Chem.*, **57**, 958 (1953).

32. H. Yamakawa and W. H. Stockmayer, *J. Chem. Phys.*, **57**, 2843 (1972).

33. J. Shimada and H. Yamakawa, *J. Chem. Phys.*, **85**, 591 (1986).

34. H. Yamakawa, "Helical Wormlike Chains in Polymer Solutions," Springer, Berlin, 1997.

35. C. Domb and A. J. Barrett, *Polymer*, **17**, 179 (1976).

36. Y. Nakamura and T. Norisuye, *J. Polym. Sci. B: Polym. Phys.*, **42**, 1398 (2004).

37. T. Konishi, T. Yoshizaki, T. Saito, Y. Einaga, and H. Yamakawa, *Macromolecules*, **23**, 290 (1990).

38. H. Yamakawa and T. Yoshizaki, *Macromolecules*, **13**, 633 (1980).

39. A. J. Barrett, *Macromolecules*, **17**, 1566 (1984).

40. P. Hickl, M. Ballauff, U. Scherf, K. Müllen, and P. Lindner, *Macromolecules*, **30**, 273 (1997).

41. K. Terao, K. Mizuno, M. Murashima, Y. Kita, C. Hongo, K. Okuyama, T. Norisuye, and H. P. Bächinger, *Macromolecules*, **41**, 7203-7210 (2008).

42. F. Kasabo, T. Kanematsu, T. Nakagawa, T. Sato, and A. Teramoto, *Macromolecules*, **33**, 2748 (2000).

43. Y. Takahashi and S. Nishikawa, *Macromolecules*, **36**, 8656 (2003).

44. C. V. Goebel, W. L. Dimpfl, and D. A. Brant, *Macromolecules*, **3**, 644 (1970).

45. J. Shimada, H. Kaneko, T. Takada, S. Kitamura, and K. Kajiwara, *J. Phys. Chem. B.*, **104**, 2136 (2000).

46. C. Yamamoto, E. Yashima, and Y. Okamoto, *J. Am. Chem. Soc.*, **124**, 12583 (2002).

Table I. Numerical results from light scattering, SAXS, viscosity, and SEC-LS measurements on ATPC samples in 1,4-dioxane (DIOX) and 2-ethoxyethanol (2EE) at 25 °C

Sample	M_w / 10^4	in DIOX				in 2EE				M_z/M_w	M_w/M_n
		$\langle S^2\rangle_z^{1/2}$ (nm)	$10^4 A_2$ ($cm^3 mol\ g^{-2}$)	$[\eta]$ ($cm^3 g^{-1}$)	k'	$\langle S^2\rangle_z^{1/2}$ (nm)	$10^4 A_2$ ($cm^3 mol\ g^{-2}$)	$[\eta]$ ($cm^3 g^{-1}$)	k'		
ATPC3M	327 [a]	99 [a]	1.4 [a]	657	0.42	82 [a]	1.2 [a]	409	0.41		
ATPC800K	76.5 [a]	44 [a]	3.0 [a]	242	0.33	36 [a]	2.3 [a]	144	0.42		1.09 [d]
ATPC500K	47.9 [a]	35 [a]	2.0 [a]	176	0.35	30 [a]	2.8 [a]	119	0.40		1.08 [d]
ATPC300K	27.9 [a]	24.5 [a]	2.2 [a]	113	0.37	22.0 [a]	3.7 [a]	83.6	0.40		1.09 [d]
ATPC200K	18.9 [a]	19.5 [a]	2.2 [a]	78.4	0.35	17.5 [a]	1.5 [a]	52.3	0.50		1.11 [d]
ATPC50K	5.48 [c]	7.8 [b]	1.3 [c]	28.6	0.43	7.3 [b]		22.9	0.83	1.05 [c]	
ATPC20K	1.87 [c]	3.3 [b]	7 [c]	10.7	0.50	3.0 [b]		8.8	1.1	1.09 [c]	

[a] Light scattering. [b] SAXS. [c] Sedimentation equilibrium. [d] SEC-LS in tetrahydrofuran at 30 °C.

Table II. Wormlike chain parameters for ATPC at 25 °C

Solvent	h (nm)	λ^{-1} (nm)	d (nm) [a]	d (nm) [b]
DIOX	0.34 ± 0.01	22 ± 2	1.3	2.9 ± 0.1
2EE	0.32 ± 0.01	16 ± 2	1.5	2.8 ± 0.1

[a] From $P(k)$. [b] From $[\eta]$.

Figure captions

Figure 1. Chemical structure of amylose tris(phenylcarbamate) (ATPC).

Figure 2. Concentration dependence of $(Kc/R_0)^{1/2}$ for indicated ATPC samples in DIOX (a) and in 2EE (b) at 25 °C.

Figure 3. Berry plots for indicated ATPC samples in DIOX (open circles) and in 2EE (filled circles) at 25 °C. (a) λ_0 = 546 nm, (b) λ_0 = 436 nm, (c) λ_0 = 0.1 nm.

Figure 4. Molecular weight dependence of $<S^2>_z^{1/2}$ and $[\eta]$ for ATPC in DIOX at 25 °C (circles), compared with earlier data by Burchard[3] (triangles) and Pfannemüller et al.[11] (squares).

Figure 5. (a) IR spectra for sample ATPC300K in mixtures of DIOX and 2EE with indicated *x* at room temperature (20 – 25 °C). (b) Difference spectra, obtained by subtracting ε in DIOX from ε for indicated *x*.

Figure 6. CD and UV spectra for sample ATPC300K in DIOX (open circles) and in 2EE (filled circles) at 25 °C.

Figure 7. Comparison between the experimental $<S^2>_z^{1/2}$ for ATPC in DIOX (open circles) and in 2EE (filled circles) both at 25 °C and the theoretical curves calculated from eq 2 for $<S^2>_0$ and the

Domb-Barrett equation[35] for α_s^2 in the QTP scheme[32-34] with M_L = 1550 nm^{-1}, λ^{-1} = 24 nm, and B = 1 nm in DIOX and M_L = 1590 nm^{-1}, λ^{-1} = 18 nm, and B = 0.8 nm in 2EE. Dashed lines show the theoretical values for B = 0.

Figure 8. Holtzer plots for ATPC50K in DIOX (a) and in 2EE (b) and for ATPC20K in DIOX (c) and in 2EE (d) at 25 °C. Solid curves, theoretical values for the unperturbed wormlike cylinder[36] with the parameters given in the text. Dashed curves, theoretical values in the rod limit ($\lambda^{-1} = \infty$).

Figure 9. Comparison between the experimental [η] for ATPC in DIOX (open circles) and in 2EE (filled circles) both at 25 °C and the theoretical curves calculated from eq 4 for $[\eta]_0$ and the Barrett equation[39] for α_η^3 in the QTP scheme with M_L = 1540 nm^{-1}, λ^{-1} = 20 nm, d = 2.9 nm, and B = 0.5 nm in DIOX and M_L = 1600 nm^{-1}, λ^{-1} = 14 nm, d = 2.8 nm, and B = 0.3 nm in 2EE. Dashed lines show the theoretical values for B = 0.

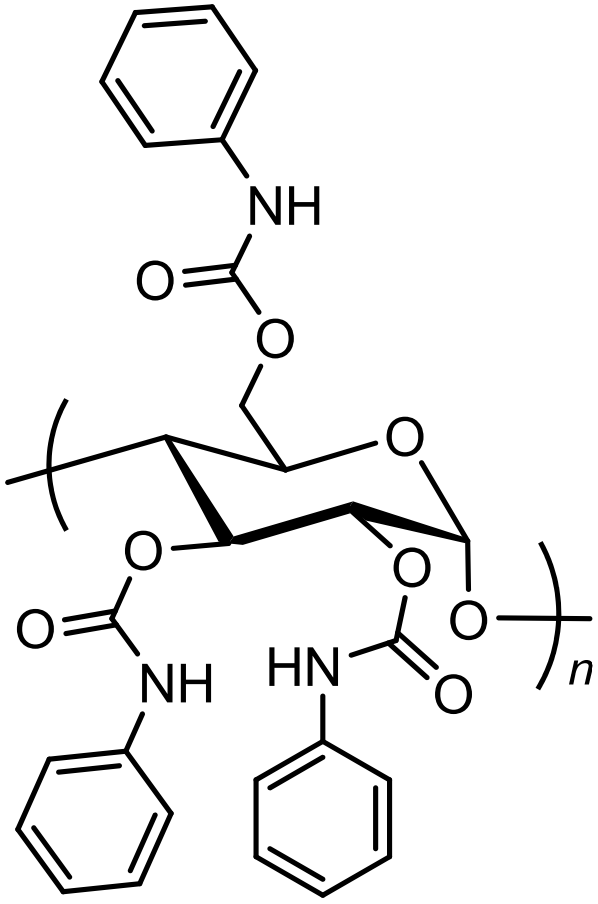

Figure 1. Terao et al.

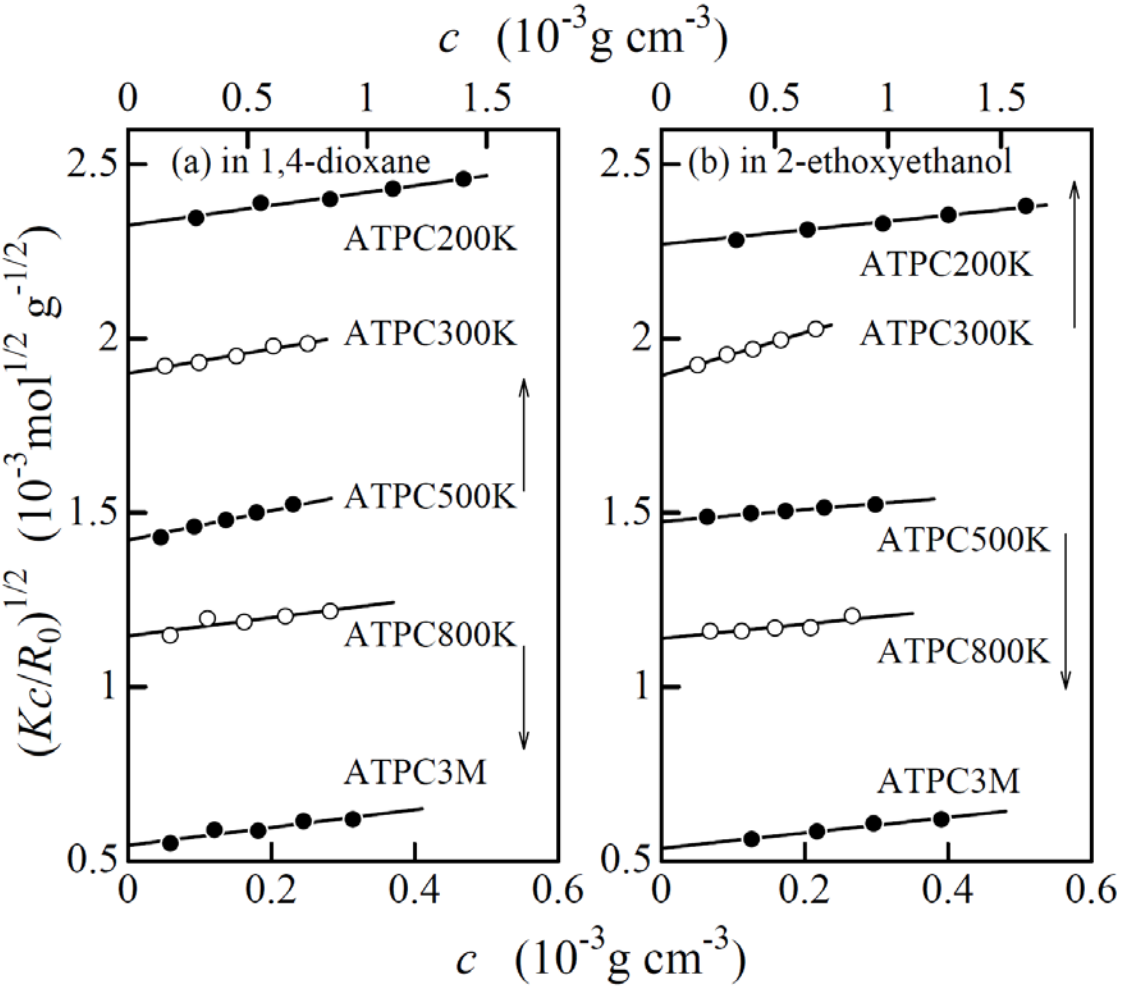

Figure 2. Terao et al.

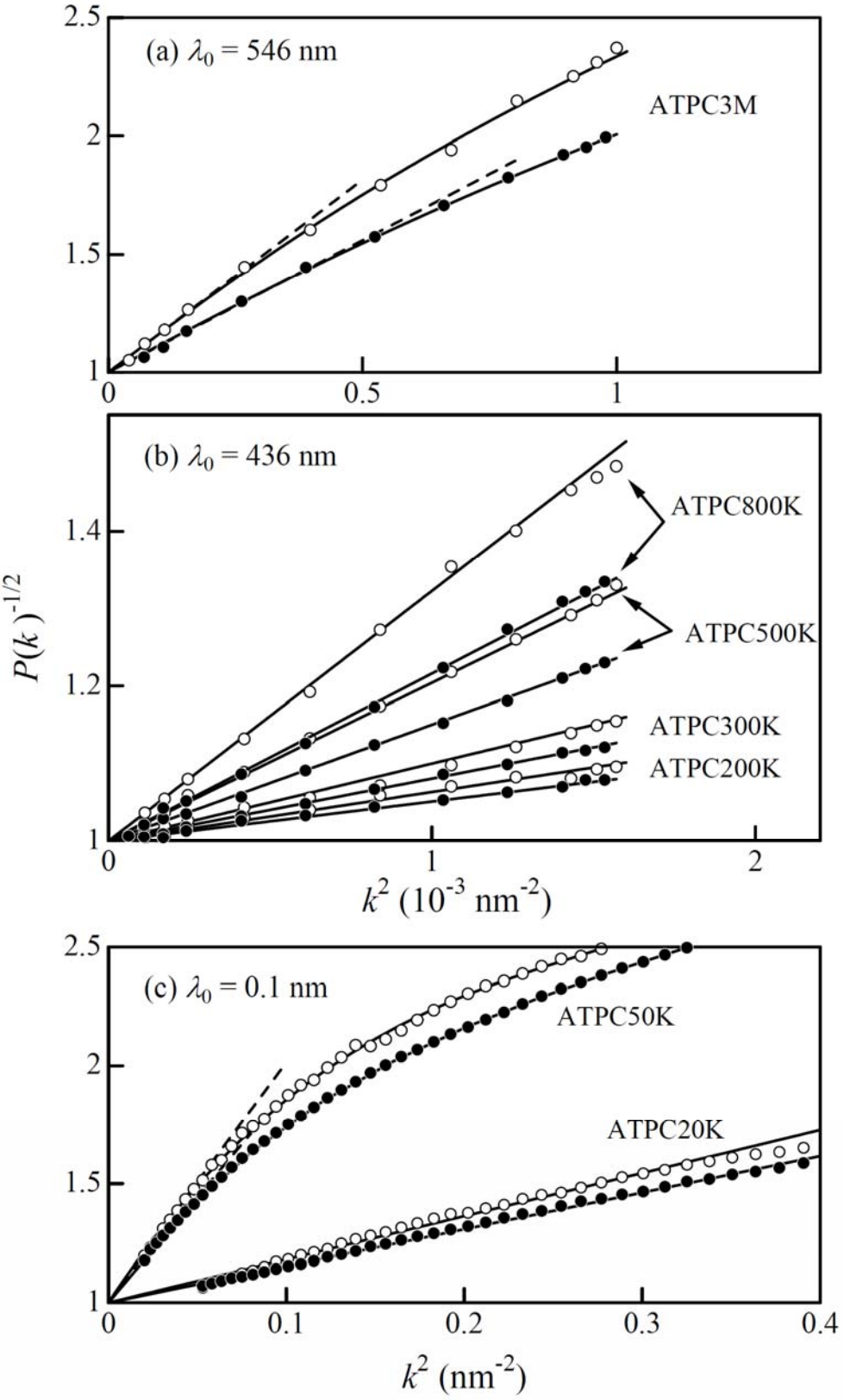

Figure 3. Terao et al.

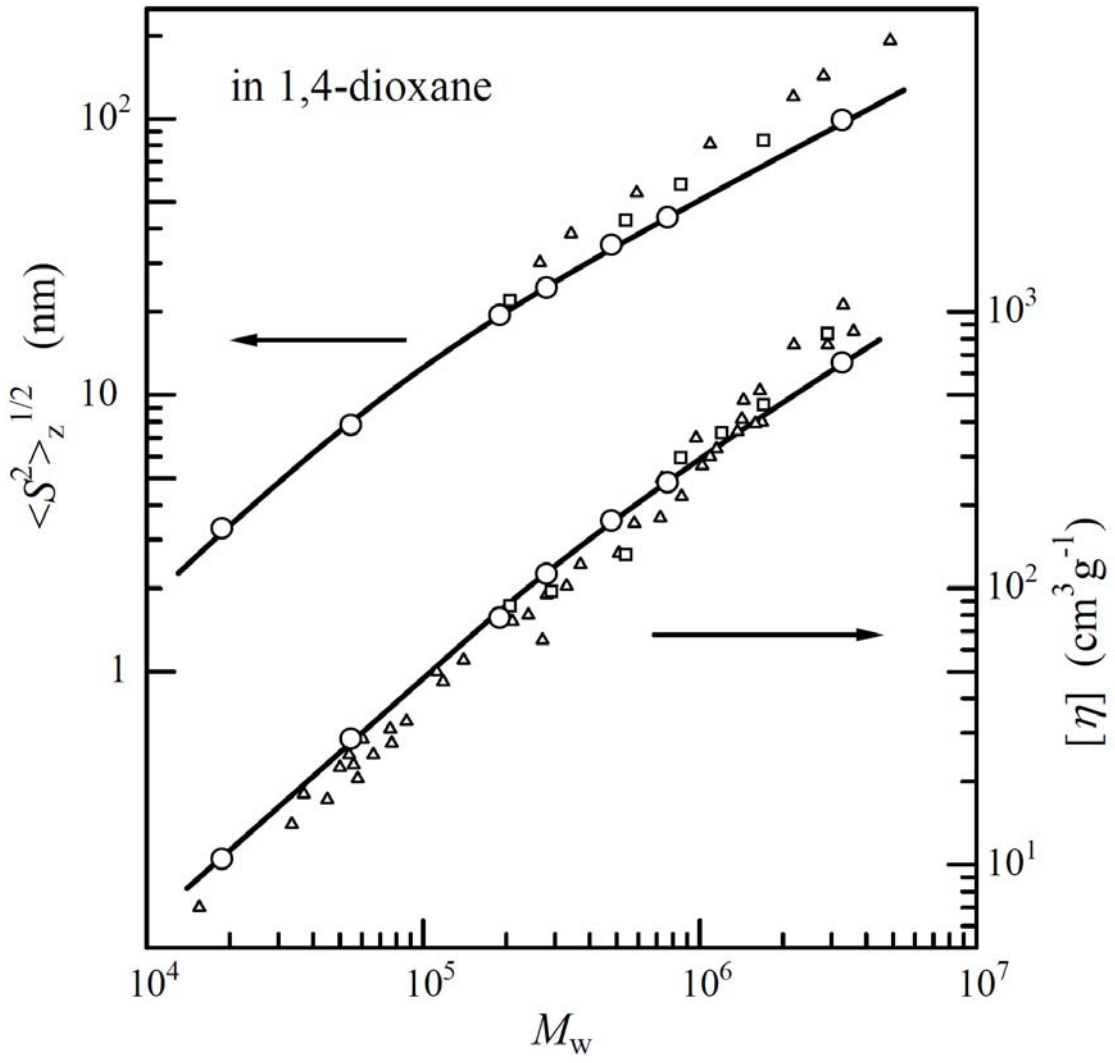

Figure 4. Terao et al.

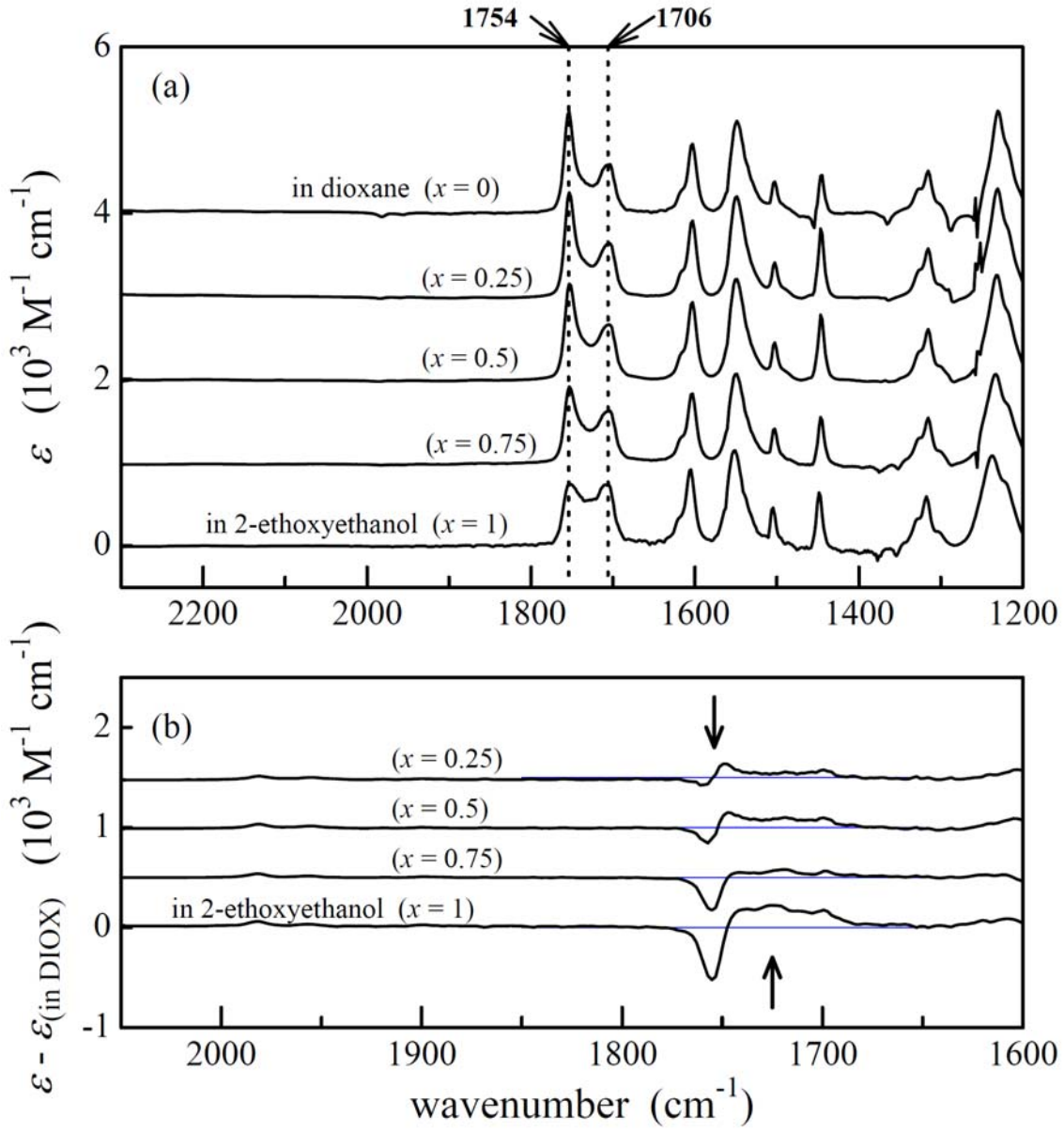

Figure 5. Terao et al.

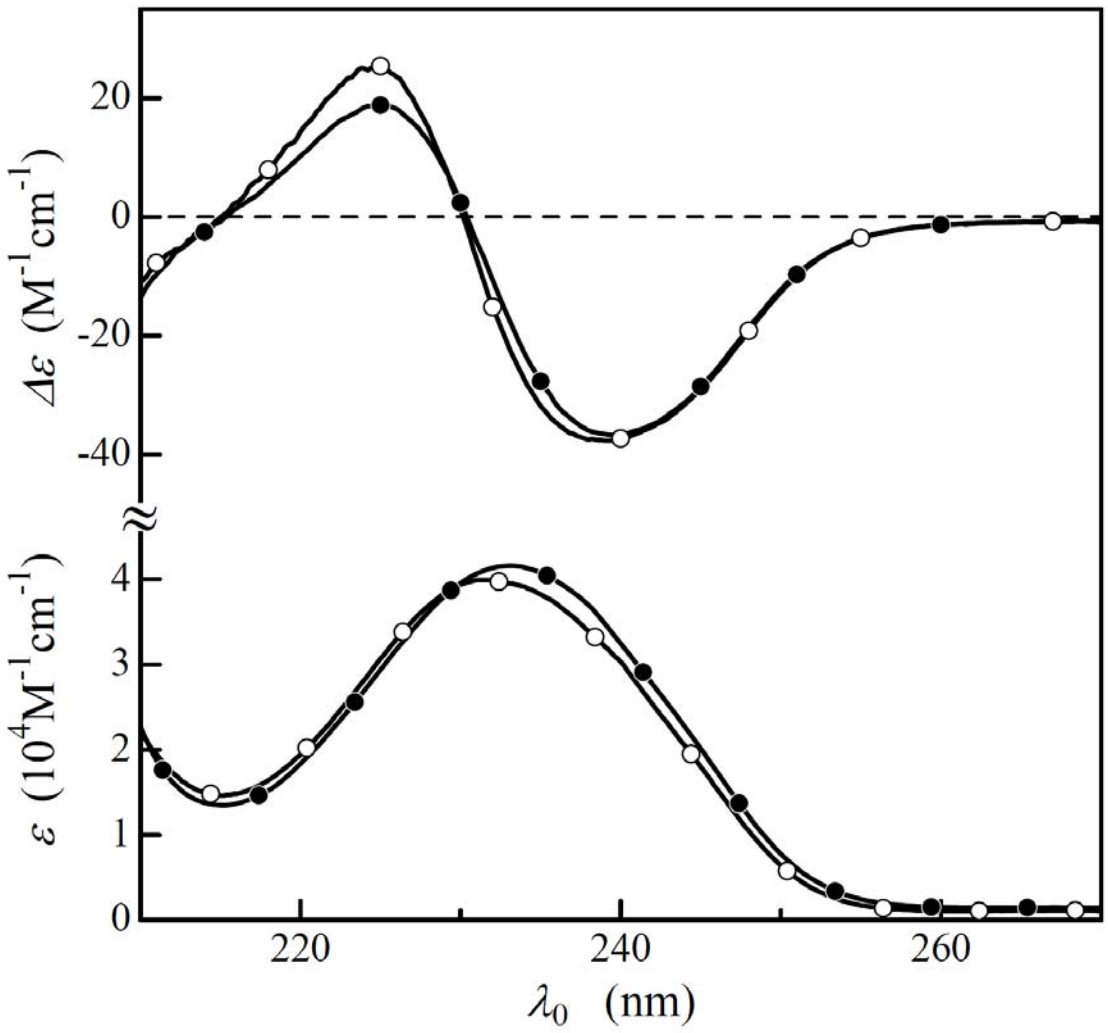

Figure 6. Terao et al.

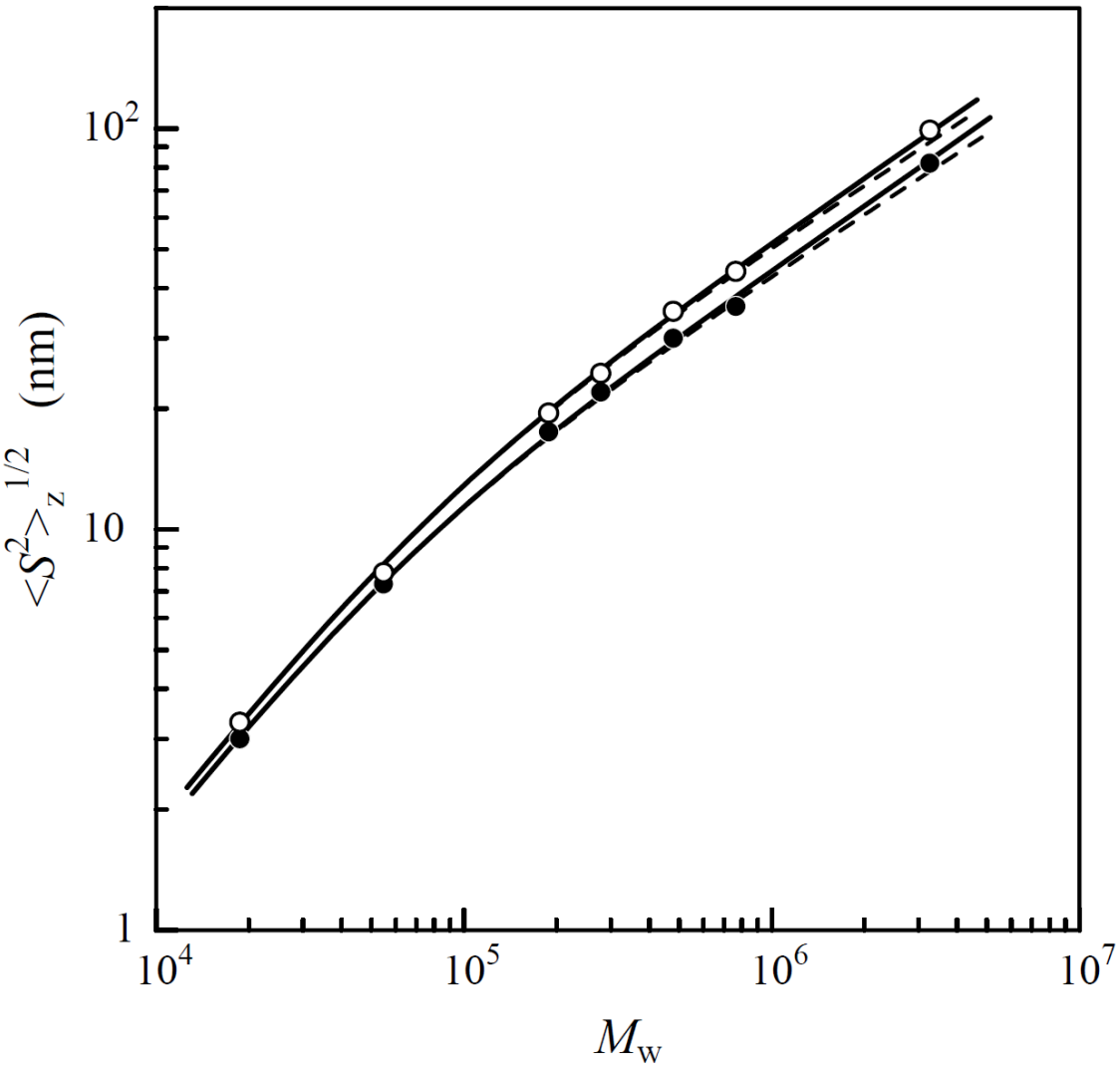

Figure 7. Terao et al.

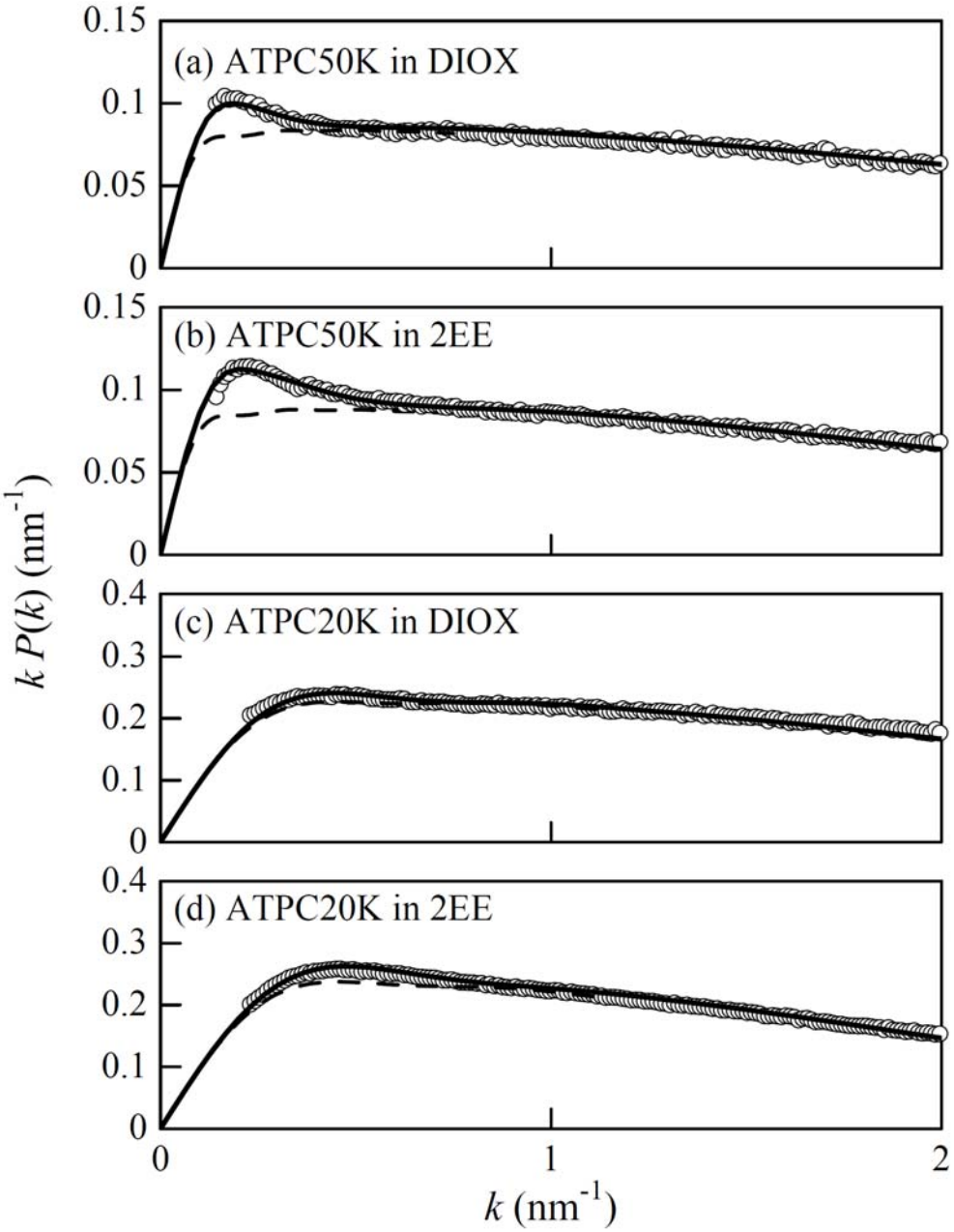

Figure 8. Terao et al.

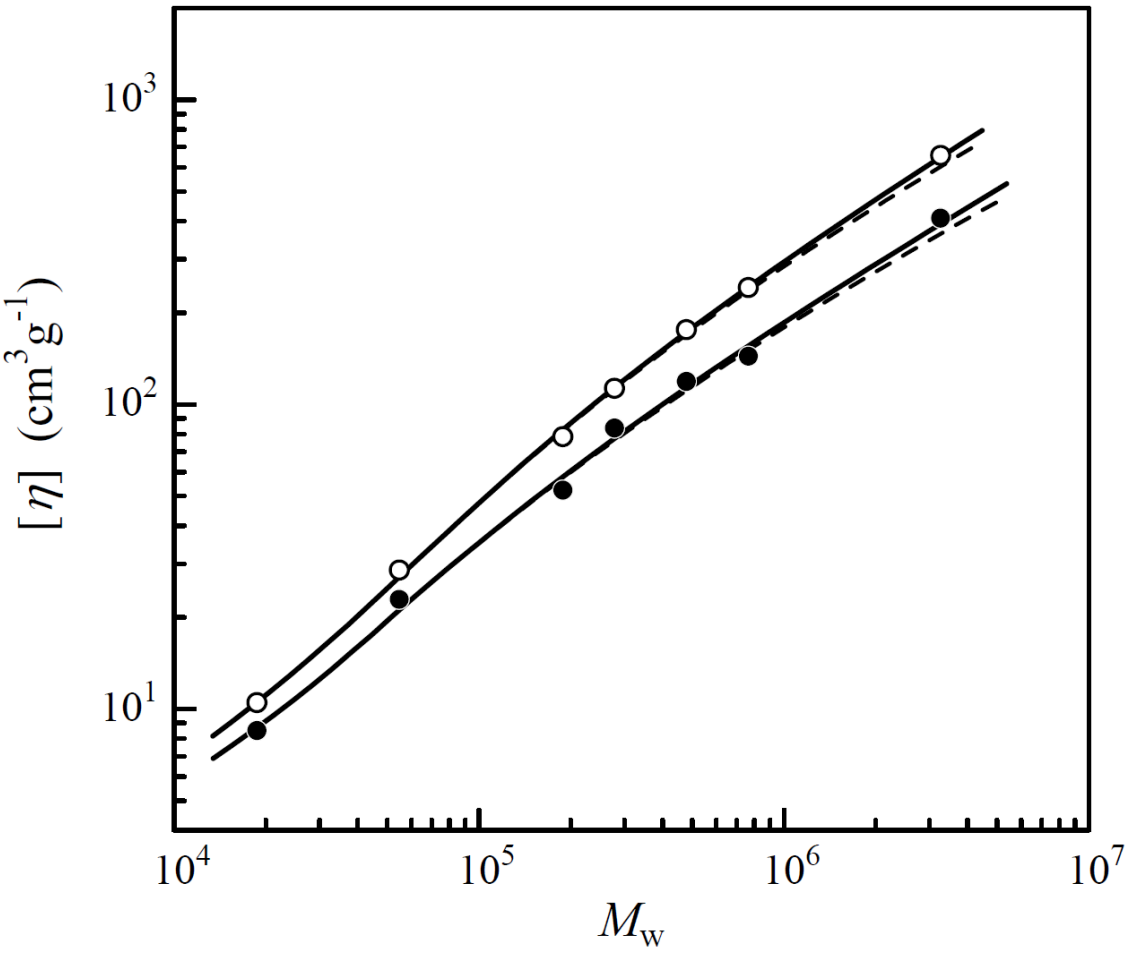

Figure 9. Terao et al.

GRAPHICAL ABSTRACT

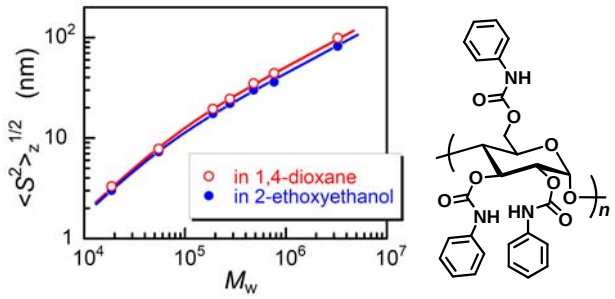

Light and small-angle X-ray scattering, sedimentation equilibrium, viscosity, circular dichroism, and infrared absorption measurements have been made on 1,4-dioxane and 2-ethoxyethanol solutions of seven amylose tris(phenylcarbamate) samples. Analyses of gyration radius, scattering function, and intrinsic viscosity data in terms of the wormlike chain model yield Kuhn segment lengths of 22 ± 2 nm and 16 ± 2 nm in 1,4-dioxane and 2-ethoxyethanol, respectively, and a contour length per residue of 0.33 ± 0.02 nm in both.